Deep Zoom-In Simulation of a Fuzzy Dark Matter Galactic Halo

Bodo Schwabe*
CAPA and Departamento de Física Teórica, Universidad de Zaragoza, 50009 Zaragoza, Spain and Institut für Astrophysik, Georg-August-Universität Göttingen, D-37077 Göttingen, Germany

Jens C. Niemeyer†
Institut für Astrophysik, Georg-August-Universität Göttingen, D-37077 Göttingen, Germany

(Received 19 October 2021; revised 4 March 2022; accepted 7 April 2022; published 2 May 2022)

Fuzzy dark matter (FDM) made of ultralight bosonic particles is a viable alternative to cold dark matter with clearly distinguishable small-scale features in collapsed structures. On large scales, it behaves gravitationally like cold dark matter deviating only by a cutoff in the initial power spectrum and can be studied using N-body methods. In contrast, wave interference effects near the de Broglie scale result in new phenomena unique to FDM. Interfering modes in filaments and halos yield a stochastically oscillating granular structure which condenses into solitonic cores during halo formation. Investigating these highly nonlinear wave phenomena requires the spatially resolved numerical integration of the Schrödinger equation. In previous papers we introduced a hybrid zoom-in scheme that combines N-body methods to model the large-scale gravitational potential around and the mass accretion onto pre-selected halos with simulations of the Schrödinger-Poisson equation to capture wave-like effects inside these halos. In this work, we present a new, substantially improved reconstruction method for the wave function inside of previously collapsed structures. We demonstrate its capabilities with a deep zoom-in simulation of a well-studied sub-L_*-sized galactic halo from cosmological initial conditions. With a particle mass of $m = 2.5 \times 10^{-22}$ eV and halo mass $M_{\rm vir} = 1.7 \times 10^{11}\ M_\odot$ in a $(60\ {\rm h}^{-1}\ {\rm comoving\ Mpc})^3$ cosmological box, it reaches an effective resolution of 20 comoving pc. This pushes the values of m and M accessible to simulations significantly closer to those relevant for studying galaxy evolution in the allowed range of FDM masses.

DOI: 10.1103/PhysRevLett.128.181301

Introduction.—Fuzzy (or wave) dark matter (FDM) is a class of ultralight bosonic dark matter models giving rise to pronounced wavelike effects in collapsed cosmological structures [1–4]. It is represented by a classical field theory for ultralight (pseudo)scalar particles, including axionlike particles, with negligible nongravitational interactions that reside in very low, highly populated momentum states. In plausible scenarios motivated by superstring cosmology [5,6], FDM particles are abundantly produced nonthermally in the early Universe. Modeled as a nonrelativistic coherent scalar field ψ with mass m their time evolution, to leading order, is governed by the comoving Schrödinger-Poisson (SP) equation [7]

$$i\hbar\frac{\partial\psi}{\partial t} = -\frac{\hbar^2}{2ma^2}\nabla^2\psi + mV\psi,$$
$$\nabla^2 V = \frac{4\pi G}{a}\delta\rho, \qquad \rho = |\psi|^2, \tag{1}$$

where V denotes the gravitational potential and a is the scale factor. The coherence wavelength $\lambda_{\rm dB} \sim \hbar/(mv)$ provides a characteristic length scale above which FDM behaves like cold dark matter (CDM) with respect to gravitational interactions [8–10], hence mirroring the successes of standard CDM on these scales.

New, discriminating phenomena occur on length scales close to $\lambda_{\rm dB}$ and characteristic times $\sim\hbar/(mv^2)$. Simulations found that FDM halos host solitonic cores surrounded by a fluctuating, granular structure formed by wave interference [2,10,11]. Later simulations started to include baryons [12,13]. Core formation [14], evolution [10,15], and mergers [16] have been further investigated. The fluctuating granules produce gravitational relaxation effects on star clusters or black holes [6,17–19] leading to strong constraints on the allowed FDM mass range [20]. Together with bounds on suppression of small-scale power from the Lyman-α forest flux power spectrum [21,22] and the high-redshift galaxy luminosity function [23–26], they indicate a lower bound on the FDM mass of $m \gtrsim 10^{-21}$ eV. For a comprehensive review see Ref. [4].

Suppression of the linear perturbation spectrum manifests itself on scales $\gg \lambda_{\rm dB}$ and is therefore accessible to standard N-body methods. On the other hand, simulations of nonlinear wavelike effects inside collapsed structures require solutions of the SP equations. These are numerically expensive since the complex phase of the wave

function has to be properly resolved in the entire simulation volume including voids [2]. Methods that solve the fluid representation of Eq. (1) including a quantum pressure term can overcome these restrictions but cannot account for interference patterns emerging after multistreaming occurs [27–30]. This approach is therefore inadequate to study wavelike effects near $\lambda\!\!\!^{-}_{\mathrm{dB}}$.

For these reasons, simulations with cosmological initial conditions and statistically meaningful volumes aiming at resolving wavelike dynamics in FDM halos have been restricted to FDM masses $m \lesssim 10^{-22}$ eV, i.e., significantly below the bound from large-scale structure probes, and halo masses $M \lesssim 10^{10}\ M_\odot$. There is an urgent need to push computational capabilities toward higher m and M with realistic initial conditions. Here, we present simulations of an isolated halo from initial conditions provided by the AGORA galaxy evolution project with final mass $M \simeq 1.7 \times 10^{11}\ M_\odot$, adapted for an FDM linear power spectrum with $m = 2.5 \times 10^{-22}$ eV. The numerical resolution needed to observe the formation of a central soliton was achieved by running deep zoom-in simulations with a hybrid N-body-Schrödinger scheme which is a significantly improved version of the method described in Ref. [10].

In Ref. [10], we combined the efficiency of N-body simulations with the accuracy of finite-difference solvers for the Schrödinger equation using adaptive mesh refinement (AMR). We conducted zoom-in simulations focusing on the inner dynamics of a few preselected halos. Evolving most of the simulation volume using N-body particles to accurately compute the large-scale gravitational field and the mass accretion onto the halos, the highly resolved halos themselves were evolved by explicitly solving the SP equations. The critical part was the reconstruction of the wave function from particle information at the N-body-Schrödinger boundaries, for which the classical wave approximation [31] was used. These simulations enabled us to investigate the dynamics of the halos' granular structure and their central solitonic cores.

The main downside of the classical wave approximation is its inability to capture the interference pattern in multistreaming regions. The wave function therefore needs to be reconstructed in the Lagrangian volume of the halo before the onset of collapse, restricting the analysis in Ref. [10] to dwarf sized halos.

In this Letter, we present a new reconstruction method for the N-body-Schrödinger boundaries that fully captures the nonlinear wave dynamics on a statistical level. It is implemented in our AXIONYX code specialized for axion-like particle dark matter simulations [32]. The new reconstruction scheme is closely related to the Gaussian beam (GB) method [33–36] originally developed for semiclassical calculations in quantum chemistry [37–42]. Variations of the GB method have been used to study the dynamics around quantum barriers with discontinuous potentials [43–45], including a hybrid method similar to the one described below [46]. It also lends itself to the analysis of interacting bosons [47] and photoexcitation and photoionization [48]. Contrary to simple ray tracing algorithms, the GB method does not become singular at caustics [34]. See the Supplemental Material [49] for details of the full GB method, its relation to our reconstruction scheme, and the implementation in AXIONYX.

Using our new GB-related technique, we can reconstruct the wave function after the preselected halo has already collapsed while resolving only the inner part of the halo well within its virial radius. This improvement enabled us to resimulate the proof-of-concept test of the AGORA High-resolution Galaxy Simulations Comparison Project [50], consisting of a dark-matter only simulation of a sub-L_*-sized galactic halo from cosmological initial conditions, with full FDM dynamics.

Simulation setup.—As part of the AGORA project [50], several widely used cosmology codes were compared by evolving identical initial conditions in a dark matter only simulation with standard ΛCDM cosmology. Using a $(60\ \mathrm{h^{-1}}\ \mathrm{comoving\ Mpc})^3$ box on a 128^3 root grid, the Lagrange patch of a preselected halo with virial mass $M \simeq 1.7 \times 10^{11}\ M_\odot$ at $z = 0$ and quiescent merger history was further resolved by five static refinement levels and up to six adaptively refining levels whenever an overdensity of four or more particles was reached in a single cell. Doubling the resolution per refinement level, the simulation was thus resolved down to 326 comoving pc. In order to properly resolve the FDM interference patterns of the preselected halo in our simulations, the wave function is reconstructed on higher levels reaching a final resolution of 20 comoving pc.

The preselected halo is first re-run in pure N-body mode with AXIONYX in order to ensure consistency with Ref. [50]. Constructing ΛCDM initial conditions at redshift $z = 100$ with MUSIC [51] as specified by the AGORA project, we recover the expected final density configuration at $z = 0$. Using the publicly available analysis scripts of the AGORA project, we obtain the same density slice plot through the halo center. The consistency of the numerical results can be seen by comparing our Fig. 1 (left) with figure 3 in Ref. [50].

FDM cosmology is characterized by a cutoff in the initial transfer function [1]. We obtained the corresponding FDM transfer function using AXIONCAMB [52] with $m = 2.5 \times 10^{-22}$ eV. Initial conditions were created with MUSIC [51], keeping the original large scale features but suppressing small scales. As expected, the N-body simulation conducted with AXIONYX reveals a final state which is effectively a smoothed version of the CDM final state. As seen in Fig. 1 (right), in the FDM run only the largest halos collapsed.

Restarting the FDM simulation at redshift $z = 3$, after the preselected halo has fully collapsed, we further refine its

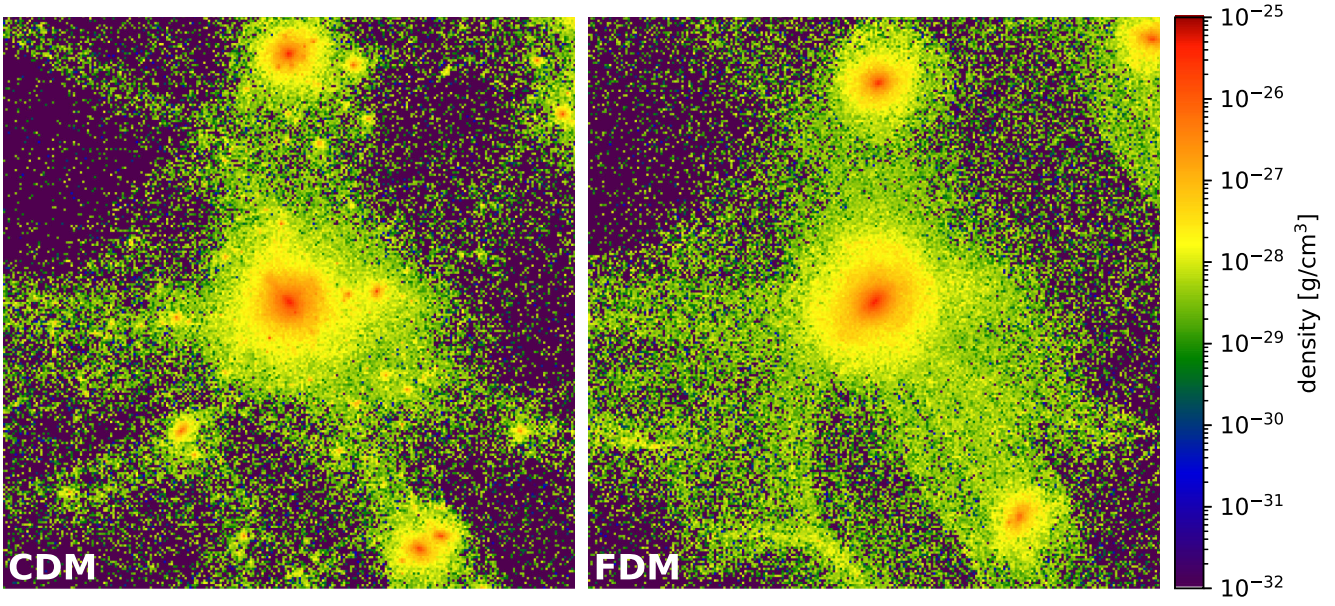

FIG. 1. N-body densities at $z = 0$ for CDM (left) and FDM (right) initial conditions of the AGORA proof-of-principle halo with virial mass $M \simeq 1.7 \times 10^{11}\ M_\odot$ in a 1 h^{-1} Mpc box. While the CDM density reproduces previous AGORA results [50], the cutoff in the FDM initial perturbation spectrum results in reduced substructure.

innermost region. After subtracting the halo's mean velocity from all particles in order to reduce resolution requirements of large phase gradients, we reconstruct the wave function on the 11th level and add three additional levels evolved by AXIONYX's finite-difference Schrödinger solver. We thus establish a hybrid method similar to the one presented in Ref. [10]. The important improvement here is the full reconstruction of the FDM interference pattern.

As the resolution of the granules on the GB level deteriorates over time, interpolation to the next finer FD level results in a continuous mass increase. We compensate for it by rescaling the wave function on the coarsest FD level such that its average density coincides with the N-body density obtained from the underlying beams. At each time step, the rescaling does not exceed a per-mil level change.

Numerical results.—Figure 2 shows density slices zoomed into the preselected halo at redshift $z = 3$. The plot on the far right depicts the wave function immediately after reconstruction. The characteristic interference pattern and the central solitonic core are clearly visible. They are refined by three additional finite-difference levels. As the collapsed halo decouples from the expanding background, its substructure shrinks relative to the simulation box. In order to ensure sufficient resolution, we insert an additional refinement level after redshift $z = 1.56$ and stop the simulation at $z = 1$.

Radial density profiles centered around the halo's density maxima at different redshifts are shown in Fig. 3. The inner region is well fitted by a solitonic core profile [2]

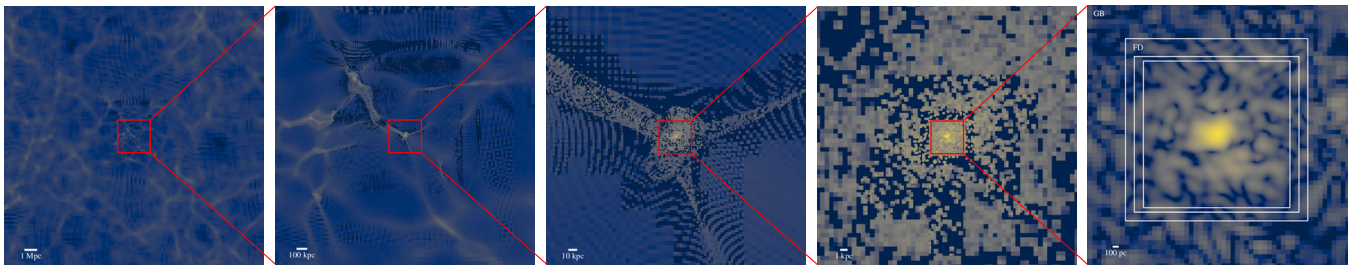

FIG. 2. Density slices zoomed into the preselected halo at redshift $z = 3$. The plot on the right shows the reconstructed wave function with self-consistent interference pattern and central solitonic core using the GB method in the innermost, highly resolved region of the halo. The wave function is evolved with an FD solver on three additional levels. Lower levels are evolved with AXIONYX's N-body solver.

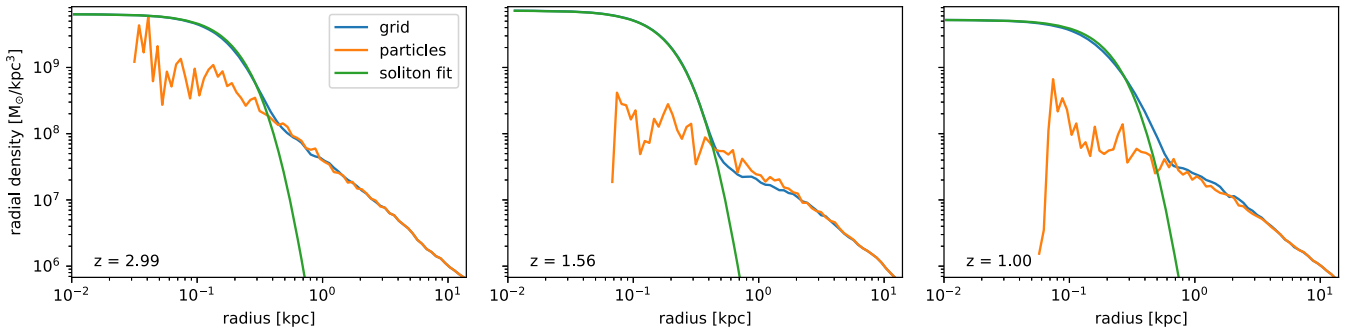

FIG. 3. Radial density profiles of the FDM wave function (blue) at different redshifts. They are well fitted by a soliton profile (green) transitioning to an outer NFW-like profile indistinguishable from the one obtain utilizing the underlying N-body particle information (orange).

$$\rho_c(r) \simeq \rho_0 \left[1 + 0.091\left(\frac{r}{r_c}\right)^2\right]^{-8}, \tag{2}$$

where r_c is the core radius at which the density has dropped to half its central value

$$\rho_0 \simeq 3.1 \times 10^6 \left(\frac{2.5 \times 10^{-22}\ \text{eV}}{m}\right)^2 \left(\frac{\text{kpc}}{r_c}\right)^4 \frac{M_\odot}{\text{kpc}^3}. \tag{3}$$

The outer angular-averaged density profile is NFW-like and statistically indistinguishable from CDM, confirming previous results.

The wave function's velocity distribution is calculated on the finest level [10]:

$$f(\mathbf{v}) = \frac{1}{N}\left|\int d^3\mathbf{x}\ \exp\left(-im\mathbf{v}\cdot\mathbf{x}/\hbar\right)\psi(\mathbf{x})\right|^2, \tag{4}$$

with normalization factor N. It was previously shown to match the underlying particle velocity distribution [10], consistent with the equivalence of the coarse-grained Schrödinger and Vlasov equations known as the Schrödinger-Vlasov correspondence [8,9,53]. As seen in Fig. 4, we recover the same similarity to the beams' velocity distribution on the finest level proving the consistency of the reconstructed interference pattern on a statistical level. Both spectra deviate from a perfect Maxwellian distribution

$$f_M(v)dv = 3\left(\frac{6}{\pi}\right)^{1/2}\frac{v^2}{v_0^3}\exp\left(-\frac{3}{2}\frac{v^2}{v_0^2}\right)dv, \tag{5}$$

with free parameter v_0 indicating that the halo has not yet reached virial equilibrium.

It was found numerically that solitonic core radii are correlated with the peaks of the velocity distributions [11,32]:

$$v_c = \frac{2\pi}{7.5}\frac{\hbar}{m r_c}. \tag{6}$$

This implies that the growth of solitons is suppressed once their virial temperature reaches that of their host halo [4,54,55] and the core-halo mass relation [2] is valid for more massive halos as well. The velocities corresponding to v_c at different redshifts are displayed as vertical lines in Fig. 4.

On average, the solitonic core's central density, depicted in Fig. 5, remains constant over the entire simulation period and oscillates on the quasi-normal frequency of the excited soliton [10,56]

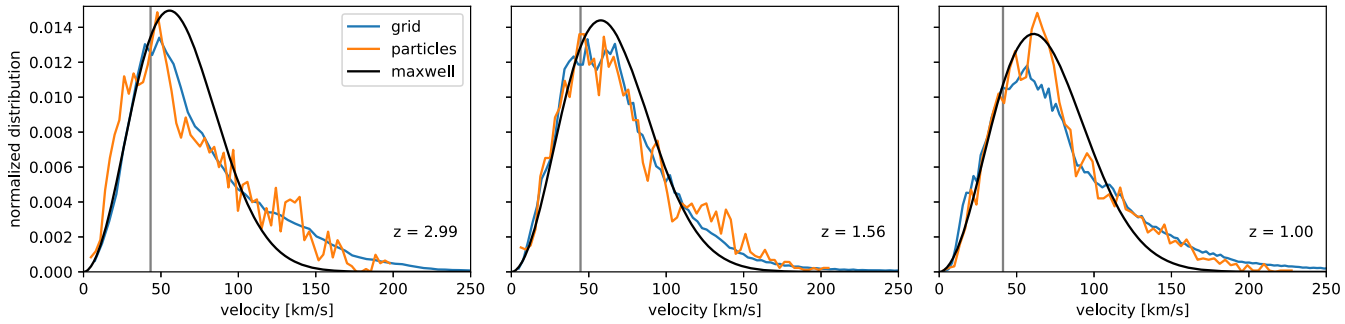

FIG. 4. Velocity spectra calculated on the finest AMR level at different redshifts. The FDM wave function's spectra (blue) are comparable to the underlying particle velocity dispersions (orange) and are close to a Maxwellian distribution (black). The vertical lines mark the velocities v_c from Eq. (6).

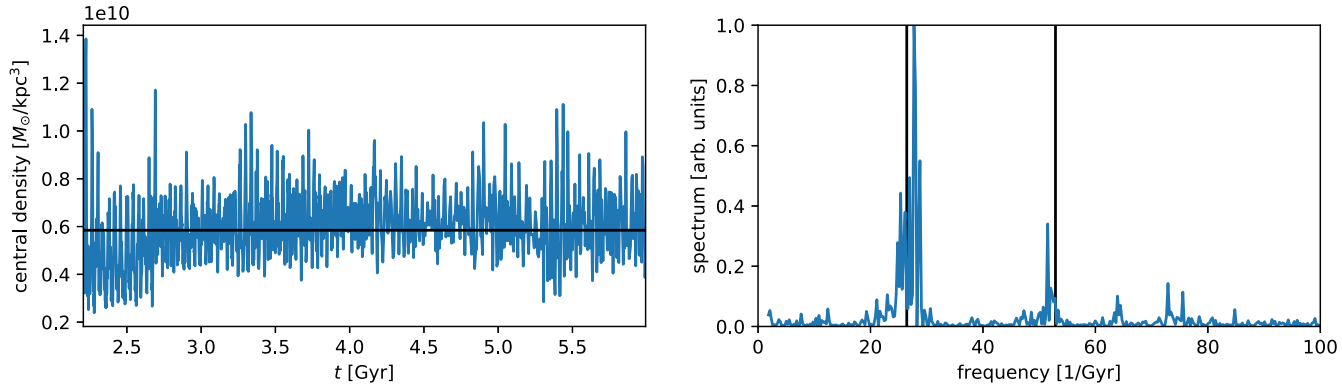

FIG. 5. (left) The central soliton density oscillates around an average value indicated by the black line. (right) Using Eq. (7) it defines a quasinormal soliton frequency and its first higher harmonic (vertical black lines), which are both well matched by the numerically obtained frequency spectrum of the oscillating central density.

$$f = 10.94\left(\frac{\rho_c}{10^9\ \mathrm{M}_\odot\ \mathrm{kpc}^{-3}}\right)^{1/2}\ \mathrm{Gyr}^{-1}. \tag{7}$$

Conclusions.—We presented the largest FDM cosmology zoom-in simulation to date with an effective resolution of 4.2×10^6 cells in all three spatial dimensions, exceeding previous FDM cosmology simulations by roughly six orders of magnitude in the number of effective grid points [2,10,57]. The spatial resolution at the highest refinement level of 20 comoving pc allowed the full wavelike simulation of a sub-L_*-sized galactic halo from cosmological initial conditions with FDM mass $m = 2.5 \times 10^{-22}$ eV.

In order to facilitate comparison with CDM, we chose to re-run the proof-of-concept dark-matter only simulation of the AGORA code comparison project [50]. We assumed standard ΛCDM cosmology in a $(60\ \mathrm{h}^{-1}$ comoving Mpc$)^3$ box with FDM initial conditions for AMR simulations of a single selected halo. Using a 128^3 root grid, the halo's Lagrange patch was further resolved by five static refinement levels and up to ten adaptively refining levels.

This deep zoom-in simulation was made possible by extending the AXIONYX code with an improved hybrid N-body-Schrödinger method building on the technique used in Refs. [10,12]. Its key advantage over full Schrödinger-Poisson simulations is the capability to solve the Schrödinger equation only in highly refined subvolumes, while relying on the Schrödinger-Vlasov correspondence to treat dark matter in regions with coarser refinement level as N-body particles. This approach drastically reduces the required spatial resolution in most of the computational volume.

The main improvement over previous versions is a new reconstruction scheme at the N-body-Schrödinger boundaries based on a simplified version of the Gaussian beam method for solving the Schrödinger equation, providing the statistically correct reconstruction of the solitonic core and the interference pattern in the central region of the collapsed halo. This methods requires only the complex phase coevolved with each N-body particle to reconstruct an FDM wave function in fully nonlinear density fields. The wave-particle conversion can therefore begin after the halo has collapsed and be confined to a region well within its virial radius.

We recover the radial FDM density profiles with a solitonic core embedded in a fluctuating halo whose averaged density profile is consistent with an NFW behavior. The FDM wave function's velocity spectrum on the finest AMR level coincides with the underlying particle velocity dispersion and resembles a Maxwellian distribution. It peaks close to the soliton's virial velocity implying that the core is in kinetic equilibrium with its surrounding. The soliton is in an exited state dominated by the quasinormal frequency mode.

Accurately modeling the oscillations of the central soliton correctly is of paramount importance for predicting the dynamics of tracers of the gravitational potential. Strong constraints on the dark matter particle mass were derived from the stability of the central star cluster subject to soliton oscillations in Eridanus II [20] and questioned by Ref. [58]. Similarly, soliton random walk caused by incoherent wave interference with the soliton is a genuinely wavelike effect with important observational consequences [59–61]. Further analysis of these effects for a variety of halo histories using our method will be the subject of future work.

Our result is a proof-of-concept demonstration of the hybrid N-body-Schrödinger method, pushing the range of m and M accessible to simulations significantly closer to those relevant for studying galaxy evolution in the allowed range of FDM masses $m \gtrsim 10^{-21}$ eV. Future simulations will need to include the effects of baryons and star formation whose strong impact on the core soliton was shown in Ref. [12]. We also expect that it will enable simulations of gravitational relaxation and heating in FDM halos from realistic initial conditions and a variety of merger histories.

Beyond FDM research, the nonlinear dynamics of the Schrödinger-Poisson equation is relevant for studying the gravitional fragmention of the inflaton field in scenarios

with early matter domination [62,63] including the formation of "inflaton stars" [64,65], as well as axion miniclusters and axion stars formed from QCD axion dark matter [54,66]. These simulations can equally benefit from the method presented here.

We thank Benedikt Eggemeier, Mateja Gosenca, and Richard Easther for important discussions. Computations described in this work were performed with resources provided by the North-German Supercomputing Alliance (HLRN). We acknowledge the yt toolkit [67] that was used for the analysis of numerical data. B. S. acknowledges support by the Deutsche Forschungsgemeinschaft and by Grant No. PGC2018-095328-B-I00(FEDER/Agencia estatal de investigación).

*bschwabe@unizar.es
†jens.niemeyer@phys.uni-goettingen.de

[1] W. Hu, R. Barkana, and A. Gruzinov, Phys. Rev. Lett. **85**, 1158 (2000).
[2] H.-Y. Schive, M.-H. Liao, T.-P. Woo, S.-K. Wong, T. Chiueh, T. Broadhurst, and W.-Y. Pauchy Hwang, Phys. Rev. Lett. **113**, 261302 (2014).
[3] D. J. Marsh, Phys. Rep. **643**, 1 (2016), axion cosmology.
[4] J. C. Niemeyer, Prog. Part. Nucl. Phys. **113**, 103787 (2020).
[5] A. Arvanitaki, S. Dimopoulos, S. Dubovsky, N. Kaloper, and J. March-Russell, Phys. Rev. D **81**, 123530 (2010).
[6] L. Hui, J. P. Ostriker, S. Tremaine, and E. Witten, Phys. Rev. D **95**, 043541 (2017).
[7] B. Salehian, H.-Y. Zhang, M. A. Amin, D. I. Kaiser, and M. H. Namjoo, J. High Energy Phys. 09 (2021) 050.
[8] L. M. Widrow and N. Kaiser, Astrophys. J. Lett. **416**, L71 (1993).
[9] C. Uhlemann, M. Kopp, and T. Haugg, Phys. Rev. D **90**, 023517 (2014).
[10] J. Veltmaat, J. C. Niemeyer, and B. Schwabe, Phys. Rev. D **98**, 043509 (2018).
[11] P. Mocz, M. Vogelsberger, V. H. Robles, J. Zavala, M. Boylan-Kolchin, A. Fialkov, and L. Hernquist, Mon. Not. R. Astron. Soc. **471**, 4559 (2017).
[12] J. Veltmaat, B. Schwabe, and J. C. Niemeyer, Phys. Rev. D **101**, 083518 (2020).
[13] P. Mocz, A. Fialkov, M. Vogelsberger, F. Becerra, M. A. Amin, S. Bose, M. Boylan-Kolchin, P.-H. Chavanis, L. Hernquist, L. Lancaster, F. Marinacci, V. H. Robles, and J. Zavala, Phys. Rev. Lett. **123**, 141301 (2019).
[14] D. G. Levkov, A. G. Panin, and I. I. Tkachev, Phys. Rev. Lett. **121**, 151301 (2018).
[15] D. D. Chowdhury, F. C. van den Bosch, V. H. Robles, P. van Dokkum, H.-Y. Schive, T. Chiueh, and T. Broadhurst, Astrophys. J. **916**, 27 (2021).
[16] B. Schwabe, J. C. Niemeyer, and J. F. Engels, Phys. Rev. D **94**, 043513 (2016).
[17] B. Bar-Or, J.-B. Fouvry, and S. Tremaine, Astrophys. J. **871**, 28 (2019).
[18] A. A. El-Zant, J. Freundlich, F. Combes, and A. Halle, Mon. Not. R. Astron. Soc. **492**, 877 (2020).
[19] L. Lancaster, C. Giovanetti, P. Mocz, Y. Kahn, M. Lisanti, and D. N. Spergel, J. Cosmol. Astropart. Phys. 01 (2020) 001.
[20] D. J. E. Marsh and J. C. Niemeyer, Phys. Rev. Lett. **123**, 051103 (2019).
[21] E. Armengaud, N. Palanque-Delabrouille, D. J. E. Marsh, J. Baur, and C. Yèche, Mon. Not. R. Astron. Soc. **471**, 4606 (2017).
[22] V. Iršič, M. Viel, M. G. Haehnelt, J. S. Bolton, and G. D. Becker, Phys. Rev. Lett. **119**, 031302 (2017).
[23] H.-Y. Schive, T. Chiueh, T. Broadhurst, and K.-W. Huang, Astrophys. J. **818**, 89 (2016).
[24] B. Bozek, D. J. E. Marsh, J. Silk, and R. F. G. Wyse, Mon. Not. R. Astron. Soc. **450**, 209 (2015).
[25] N. Menci, A. Merle, M. Totzauer, A. Schneider, A. Grazian, M. Castellano, and N. G. Sanchez, Astrophys. J. **836**, 61 (2017).
[26] P. S. Corasaniti, S. Agarwal, D. J. E. Marsh, and S. Das, Phys. Rev. D **95**, 083512 (2017).
[27] P. Mocz and S. Succi, Phys. Rev. E **91**, 053304 (2015).
[28] J. Veltmaat and J. C. Niemeyer, Phys. Rev. D **94**, 123523 (2016).
[29] M. Nori and M. Baldi, Mon. Not. R. Astron. Soc. **478**, 3935 (2018).
[30] P. F. Hopkins, Mon. Not. R. Astron. Soc. **489**, 2367 (2019).
[31] C. Trahan and R. Wyatt, *Quantum Dynamics with Trajectories: Introduction to Quantum Hydrodynamics*, Interdisciplinary Applied Mathematics (Springer, New York, 2005).
[32] B. Schwabe, M. Gosenca, C. Behrens, J. C. Niemeyer, and R. Easther, Phys. Rev. D **102**, 083518 (2020).
[33] E. Kluk, M. F. Herman, and H. L. Davis, J. Chem. Phys. **84**, 326 (1986).
[34] K. G. Kay, J. Chem. Phys. **100**, 4377 (1994).
[35] A. Bach, *An Introduction to Semiclassical and Microlocal Analysis*, Universitext (Springer, New York, 2002).
[36] K. G. Kay, Chem. Phys. **322**, 3 (2006).
[37] M. Ceotto, G. Di Liberto, and R. Conte, Phys. Rev. Lett. **119**, 010401 (2017).
[38] A. Patoz, T. Begušić, and J. Vaníček, J. Phys. Chem. Lett. **9**, 2367 (2018).
[39] M. Buchholz, F. Grossmann, and M. Ceotto, J. Chem. Phys. **148**, 114107 (2018).
[40] G. Bertaina, G. Di Liberto, and M. Ceotto, J. Chem. Phys. **151**, 114307 (2019).
[41] F. Gabas, G. Di Liberto, and M. Ceotto, J. Chem. Phys. **150**, 224107 (2019).
[42] T. Begušić, M. Cordova, and J. Vaníček, J. Chem. Phys. **150**, 154117 (2019).
[43] K. G. Kay, Phys. Rev. A **88**, 012122 (2013).
[44] S. Jin, D. Wei, and D. Yin, J. Comput. Appl. Math. **265**, 199 (2014), Current Trends and Progresses in Scientific Computation.
[45] J. Lu and Z. Zhou, J. Chem. Phys. **145**, 124109 (2016).
[46] P. Q. Shi Jin, Kinet. Relat. Models **4**, 1097 (2011).
[47] S. Ray, P. Ostmann, L. Simon, F. Grossmann, and W. T. Strunz, J. Phys. A **49**, 165303 (2016).
[48] A. B. Bichkov and V. V. Smirnov, J. Phys. Conf. Ser. **635**, 092056 (2015).
[49] See Supplemental Material at http://link.aps.org/supplemental/10.1103/PhysRevLett.128.181301 for details

regarding the full GB method, its relation to our reconstruction scheme (Sec. S1), and the implementation in AXIONYX (Sec. S2).

[50] J.-h. Kim *et al.* (AGORA Collaboration29), Astrophys. J. Suppl. Ser. **210**, 14 (2014).

[51] O. Hahn and T. Abel, Mon. Not. R. Astron. Soc. **415**, 2101 (2011).

[52] R. Hlozek, D. Grin, D. J. E. Marsh, and P. G. Ferreira, Phys. Rev. D **91**, 103512 (2015).

[53] P. Mocz, L. Lancaster, A. Fialkov, F. Becerra, and P.-H. Chavanis, Phys. Rev. D **97**, 083519 (2018).

[54] B. Eggemeier and J. C. Niemeyer, Phys. Rev. D **100**, 063528 (2019).

[55] J. Chen, X. Du, E. W. Lentz, D. J. E. Marsh, and J. C. Niemeyer, Phys. Rev. D **104**, 083022 (2021).

[56] F. S. Guzman and L. A. Urena-Lopez, Phys. Rev. D **69**, 124033 (2004).

[57] S. May and V. Springel, Mon. Not. R. Astron. Soc. **506**, 2603 (2021).

[58] B. T. Chiang, H.-Y. Schive, and T. Chiueh, Phys. Rev. D **103**, 103019 (2021).

[59] H.-Y. Schive, T. Chiueh, and T. Broadhurst, Phys. Rev. Lett. **124**, 201301 (2020).

[60] D. Dutta Chowdhury, F. C. van den Bosch, V. H. Robles, P. van Dokkum, H.-Y. Schive, T. Chiueh, and T. Broadhurst, Astrophys. J. **916**, 27 (2021).

[61] X. Li, L. Hui, and T. D. Yavetz, Phys. Rev. D **103**, 023508 (2021).

[62] N. Musoke, S. Hotchkiss, and R. Easther, Phys. Rev. Lett. **124**, 061301 (2020).

[63] B. Eggemeier, J. C. Niemeyer, and R. Easther, Phys. Rev. D **103**, 063525 (2021).

[64] J. C. Niemeyer and R. Easther, J. Cosmol. Astropart. Phys. 07 (2020) 030.

[65] B. Eggemeier, B. Schwabe, J. C. Niemeyer, and R. Easther, Phys. Rev. D **105**, 023516 (2022).

[66] B. Eggemeier, J. Redondo, K. Dolag, J. C. Niemeyer, and A. Vaquero, Phys. Rev. Lett. **125**, 041301 (2020).

[67] M. J. Turk, B. D. Smith, J. S. Oishi, S. Skory, S. W. Skillman, T. Abel, and M. L. Norman, Astrophys. J. Suppl. Ser. **192**, 9 (2011).